

Pitfalls in using statistical bias-correction methods to characterize climate change impacts

Nicolás A. Vásquez¹, Pablo A. Mendoza^{1,2}, Wouter J. M. Knoben^{3*}, Louise Arnal^{3†}, Miguel Lagos-Zúñiga⁴, Martyn Clark^{3‡}, Ximena Vargas¹

¹Department of Civil Engineering, Universidad de Chile

²Advanced Mining Technology Center, Universidad de Chile

³Centre for Hydrology, University of Saskatchewan, Canmore, Alberta, Canada

⁴Center for Climate and Resilience Research, Universidad de Chile

Key Points:

- The choice of temporal stratification for GCM bias correction is crucial for removing biases, even for GCMs with good raw seasonality.
- Different temporal stratifications used for GCM bias correction may yield different future seasonalities and signals in projected changes.
- The scaling factor method is effective to assess if the temporal stratification affects the precipitation seasonality projected by a GCM.

*now at the Department of Civil Engineering, Schulich School of Engineering, University of Calgary, Calgary, Alberta, Canada

†now at Ouranos, Montreal, Quebec, Canada

‡now at the Department of Civil Engineering, Schulich School of Engineering, University of Calgary, Calgary, Alberta, Canada

Corresponding author: Nicolás A. Vásquez, nicolas.vasquez.pl@uchile.cl

Abstract

Characterizing climate change impacts on water resources typically relies on Global Climate Model (GCM) outputs that are bias-corrected using observational datasets. In this process, two pivotal decisions are (i) the Bias Correction Method (BCM) and (ii) how to handle the historically observed time series, which can be used as a continuous whole (i.e., without dividing it into sub-periods), or partitioned into monthly, seasonal (e.g., three months), or any other temporal stratification (TS). Here, we examine how the interplay between the choice of BCM, TS, and the raw GCM seasonality may affect historical portrayals and projected changes. To this end, we use outputs from 29 GCMs belonging to the CMIP6 under the Shared Socioeconomic Pathway 5–8.5 scenario, using seven BCs and three TSs (entire period, seasonal, and monthly). The results show that the effectiveness of BCs in removing biases can vary depending on the TS and climate indices analyzed. Further, the choice of BCM and TS may yield different projected change signals and seasonality (especially for precipitation), even for climate models with low bias and a reasonable representation of precipitation seasonality during a reference period. Because some BCs may be computationally expensive, we recommend using the linear scaling method as a diagnostics tool to assess how the choice of TS may affect the projected precipitation seasonality of a specific GCM. More generally, the results presented here unveil trade-offs in the way BCs are applied, regardless of the climate regime, urging the hydroclimate community for a careful implementation of these techniques.

Plain Language Summary

Global Climate Models (GCMs) are useful tools to characterize the historical and future evolution of the Earth's climate and its impacts on water resources. Because these models contain errors and their horizontal resolution is too coarse for local impact assessments, spatial downscaling and bias correction are required steps. In particular, bias correction methods can be trained and applied using all the available historical data or by splitting the time series (e.g., by season or months). Since there is no guideline on selecting a temporal stratification, we analyze bias-corrected GCM outputs obtained with three types of strategy (entire period, seasons, and months) and seven bias-correction techniques over continental Chile. We show that the choice of bias correction method and the temporal stratification applied can modify the projected precipitation signal and seasonality. We also propose a simple statistical technique to identify if, for a given climate model, the temporal stratification may be a relevant decision for climate impact assessments.

1 Introduction

Understanding and quantifying climate change impacts is crucial for long-term water resources planning and management. Such characterization typically involves hydrologic model simulations forced by an ensemble of scenario-driven meteorological time series obtained from Statistically Downscaled Bias-Corrected (SDBC) Global Climate Model (GCM) outputs (e.g., Addor et al., 2014; Hattermann et al., 2018; Her et al., 2019; Chen et al., 2021; Hanus et al., 2021; Vicuña et al., 2021). This approach usually requires the choice of emission scenario (e.g., Vano et al., 2015; Chegwiddden et al., 2019), the choice of GCM (e.g., Hakala et al., 2018; Di Virgilio et al., 2022), the selection of Bias Correction Method (BCM) (e.g., Werner & Cannon, 2016; Gutiérrez et al., 2019; Hess et al., 2023), and the choice of observational (or reference) dataset (e.g., Wootten et al., 2021; Rastogi et al., 2022).

Among the above decisions, the selection and configuration of BCs is a critical step given the risk of introducing artificial perturbations in GCM outputs (Hagemann et al., 2011; Maurer & Pierce, 2014; Wootten et al., 2021), generating a mismatch between simulated (i.e., obtained from bias-corrected GCMs) and observed (i.e., obtained

66 from a reference dataset) annual cycles of climate variables (e.g., precipitation; Teutschbein
67 & Seibert, 2010; Alder & Hostetler, 2019; Chen et al., 2021), with potential effects on
68 projected climate change impacts and subsequent interpretations and adaptation strate-
69 gies. A somewhat overlooked step is the strategy for handling the time series when ap-
70 plying BCMs, hereafter referred to as temporal stratification (TS). For example, the bias
71 correction of simulated daily time series can be performed using all the historical period
72 (i.e., a single application of the BCM; e.g., Ghimire et al., 2019) or sub-periods of the
73 historical time series, such as seasons (e.g., four applications of the BCM; e.g., Ruffault
74 et al., 2014; Teng et al., 2015), months (i.e., twelve applications of the BCM; e.g., Pierce
75 et al., 2015; Switanek et al., 2017; Matiu & Hanzer, 2022; Wu et al., 2022; J. Guo et al.,
76 2023), or any other temporal window (e.g., Haerter et al., 2011; Reiter et al., 2018).

77 Despite the large body of work exploring modeling decisions at the top of the ‘cas-
78 cade of uncertainty’ (Wilby & Dessai, 2010), climate impact studies have typically re-
79 lied on subjectively selected TSs. For example, Teng et al. (2015) compared four BCMs
80 (applied with a seasonal TS) for hydrological projections in southeastern Australia, con-
81 cluding that the hydrological model amplifies biases in precipitation after applying the
82 BCMs, and that the large spread in the projected signal of changes in precipitation ex-
83 tremes yields different impacts on runoff. Hakala et al. (2018) applied the quantile map-
84 ping (QM) method (using a seasonal TS) to assess whether a hydrological model, forced
85 by SDBC GCMs, can replicate the hydrological climatology observed during a histor-
86 ical reference period, obtaining that, even after bias correction, biases in precipitation
87 and streamflow seasonality persist. To analyze the effects of different observational datasets
88 and BCMs on climate projections, Wootten et al. (2021) used three observational datasets
89 to apply two BCMs: (i) the ‘Delta’ approach with a 3-month moving window, and (ii)
90 the quantile delta mapping (QDM) method over four periods consisting of three non-
91 overlapping months. They concluded that the selection of BCMs and observational datasets
92 have different impacts on historical and projected time series for different variables, al-
93 though they did not isolate the effect of the TS.

94 Other studies have focused on the ability of different BCMs to reproduce histor-
95 ically observed climate indices (e.g., Gutmann et al., 2014; François et al., 2020; Xavier
96 et al., 2022), or the effects on climate projections (e.g., Maurer & Pierce, 2014; Melsen
97 et al., 2018), without emphasizing the role of the TS and the evaluation timescale. More
98 recently, Vogel et al. (2023) proposed a framework to evaluate downscaling and BCMs
99 for climate change studies and demonstrated it over Australia using four GCMs, three
100 BCMs and two downscaling methods, considering different TS (monthly, 3-month, and
101 multi-time scales) for the BCMs. They suggested that the TS may influence the anal-
102 ysis (after bias correction) and should be adequately chosen after a careful bias assess-
103 ment.

104 Although the preceding studies have covered domains with specific climate types,
105 the trade-offs in selecting TS, BCMs, and GCMs for estimating historical biases (after
106 applying BCMs) and projections across contrasting climates remain unclear. Hence, this
107 paper seeks to disentangle the relative contribution of these decisions (especially TS) to
108 the spread of bias-corrected time series at the annual, seasonal, and monthly timescales
109 during historical and future periods rather than finding the ‘best’ configuration for the
110 assessment of climate change impacts. Specifically, we address the following research ques-
111 tions:

- 112 1. To what extent does the choice of bias correction method and temporal stratifi-
113 cation alter historical GCM simulations across different climate regions?
- 114 2. What are the effects of bias correction methods and temporal stratification on the
115 projected signal and seasonality of different climate variables?

- 116 3. Are there any connections between the effects of TS (on historical biases and pro-
 117 jections) and the capability of raw GCM output to replicate historically observed
 118 climatology?

119 To seek answers, we evaluate the performance of 29 SDBC GCMs from the sixth phase
 120 of the Coupled Models Intercomparison Project (CMIP6; O'Neill et al., 2016) over dif-
 121 ferent climate groups in continental Chile. We use seven methods (three univariate and
 122 four multivariate) to correct biases in precipitation and maximum and minimum tem-
 123 perature. All BCs are applied at three different TSs: (i) using the entire period (i.e.,
 124 all daily data simultaneously used for one application of the BCM), (ii) seasonally (i.e.,
 125 four applications of the BCM using four seasonally stratified time series), and (iii) monthly
 126 (i.e., twelve applications of the BCM for twelve monthly stratified time series).

127 2 Study area and datasets

128 2.1 Study area

129 Our study domain is continental Chile, which is suitable for a comprehensive as-
 130 sessment of the TS-BCM-GCM interplay in very different climate types. Figure 1 shows
 131 the spatial distribution of mean annual precipitation, mean annual temperature, and three
 132 climate indices. The snowfall fraction $SF = Sn/P$ (Figure 1d) is the fraction of mean
 133 annual precipitation (P , Figure 1b) falling as snow (Sn). The aridity index (Figure 1e)
 134 is the ratio between mean annual potential evapotranspiration (PET) and mean annual
 135 precipitation. Finally, the precipitation seasonality (p-seasonality, Figure 1f) indicates
 136 whether most precipitation falls during winter (negative values) or summer (positive val-
 137 ues). In this paper, we use the season names within the context of the Southern Hemi-
 138 sphere (i.e., winter refers to months JJA, while summer to DJF).

139 In the northern area (17°S-25°S), two main climate zones can be identified: (i) the
 140 super-arid coastal area, with very low annual precipitation amounts (<50 mm/yr), and
 141 (ii) the Altiplano region, with lower temperatures due to increasing altitude and larger
 142 annual precipitation (~200 mm/yr). The mean annual precipitation increases towards
 143 the south, although the Andes Cordillera generates a west-east gradient, with larger pre-
 144 cipitation amounts and lower temperatures on the western slopes of the Andes Cordillera
 145 compared to the valleys. Moving south from ~37°S, the altitude of Andean mountains
 146 progressively decreases, as well as the contribution of snowmelt to runoff, whereas pre-
 147 cipitation increases. South from 45°S, a west-to-east precipitation gradient produces high
 148 precipitation amounts on the coast (>2500 mm/yr), whereas a dry climate develops in
 149 Patagonia a few kilometers to the east, with decreasing precipitation amounts. In sum-
 150 mary: (i) most snowfall occurs in the Andes Cordillera, though snowfall events can also
 151 occur in the valleys of Austral Chile (<45°S); (ii) the hydroclimate is water-limited ($PET/P >$
 152 1) in approximately half of the Chilean territory, especially from ~35°S to the north, whereas
 153 the hydroclimate of the south is energy limited ($PET/P < 1$); and (iii) most precipi-
 154 tation in Chile falls during the winter (red color in panel f), being the Altiplano (north-
 155 ern Chile) and Patagonia (~50-55°S) two notable exceptions. For a more comprehen-
 156 sive review of the climate and weather of Chile, readers are referred to Aceituno et al.
 157 (2021) and Vásquez et al. (2021).

158 2.2 Datasets

159 We use the gridded meteorological product CR2MET v2.5 (Boisier et al., 2018; DGA,
 160 2022) as the observational baseline (hereafter reference dataset). CR2MET precipita-
 161 tion estimates (pr) are obtained through a combination of (i) logistic regression mod-
 162 els and (ii) multiple linear regression models that use ERA5 reanalysis outputs (Hersbach
 163 et al., 2020) and geomorphological attributes as predictors and daily precipitation from
 164 meteorological stations as predictands. For daily extreme temperatures (tmax and tmin),

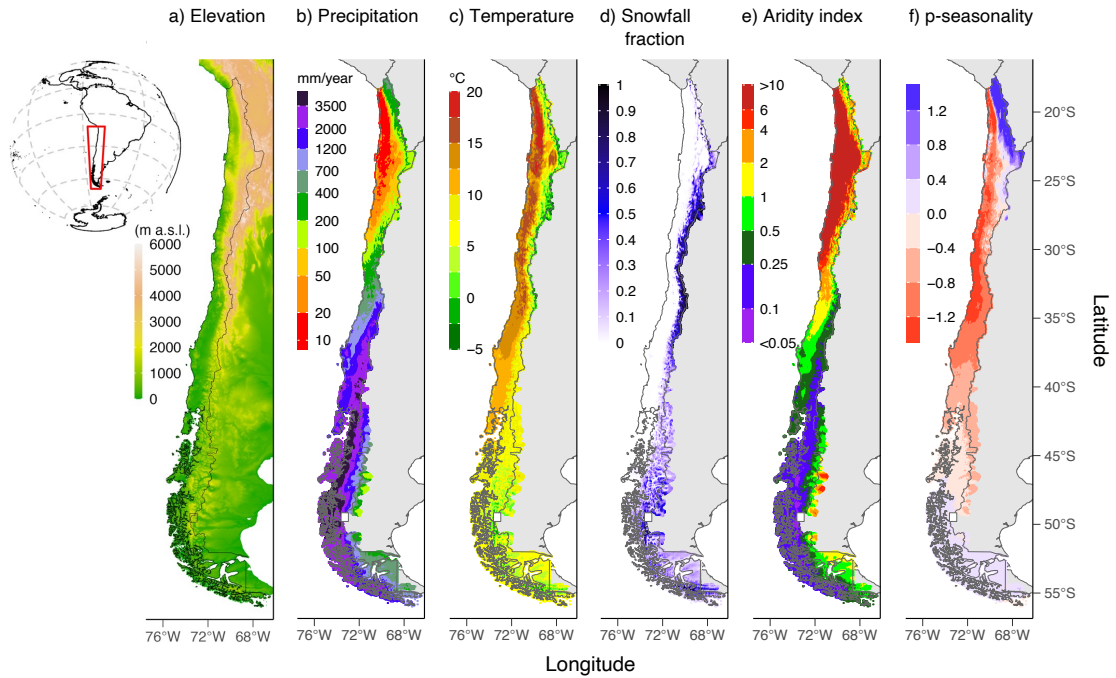


Figure 1. Main physiographic and climate attributes of continental Chile for the period 1980-2014 (34 water years): (a) elevation, (b) mean annual precipitation, (c) mean annual temperature, (d) snowfall fraction, (e) aridity index, and (f) p-seasonality.

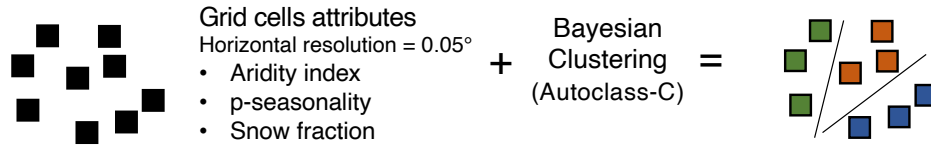
165 land surface temperature from MODIS AQUA and TERRA (Wan, 2014) are also included
 166 as predictors. All variables (pr, tmax, and tmin) are available at a daily time step for
 167 the period January/1979-March/2020, covering continental Chile at a horizontal reso-
 168 lution of $0.05^\circ \times 0.05^\circ$. The mean daily temperature is computed as the average between
 169 tmax and tmin. It should be noted that CR2MET is, arguably, the most accurate me-
 170 teorological dataset for continental Chile since its development incorporated local me-
 171 teorological stations.

172 We use outputs from 29 GCMs from the CMIP6 (O'Neill et al., 2016), based on
 173 the data availability for pr, tmax and tmin during the historical and projected periods,
 174 and the SSP5-8.5 scenario for being the worst in terms of greenhouse emissions and the
 175 'business as usual' development case. The name and horizontal resolution of each GCM
 176 are included in Table A1.

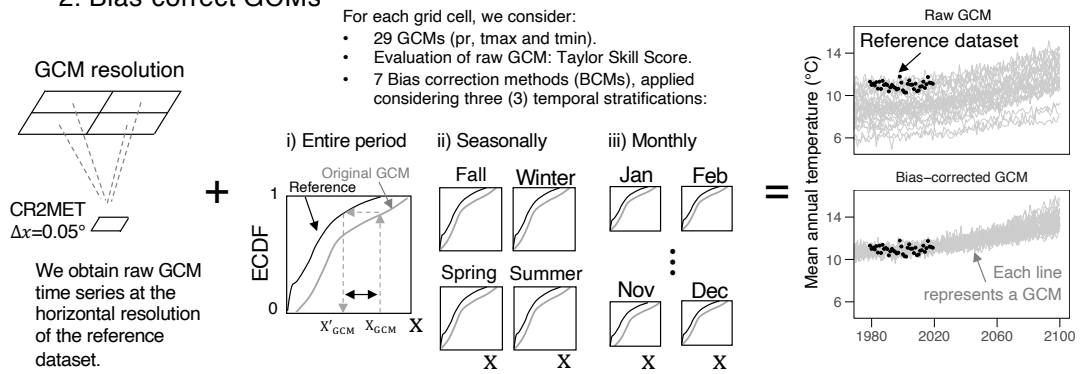
177 3 Methodology

178 Figure 2 shows the main steps of our approach. First, we delineate climate zones
 179 across Chile using cluster analysis (step 1), with the aim to examine possible relation-
 180 ships between climate types and the BCM-TS-GCM interplay. Step 2 considers differ-
 181 ent strategies for correcting biases in GCM outputs (i.e., seven bias-correction methods
 182 are applied using three different stratification periods). In step 3, we compute several
 183 climate indices derived from precipitation and temperature at different time scales (e.g.,
 184 annual, seasonal, and monthly mean values), for a historical and a future period. Finally,
 185 we conduct an Analysis of Variance (ANOVA) to quantify the relative contribution of
 186 different decisions to the spread of historical estimates. More details can be found in the
 187 following sections.

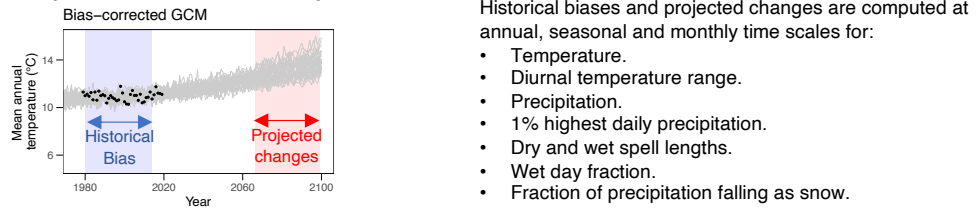
1. Climate clustering



2. Bias-correct GCMs



3. Compute metrics from daily time series



4. ANOVA analysis

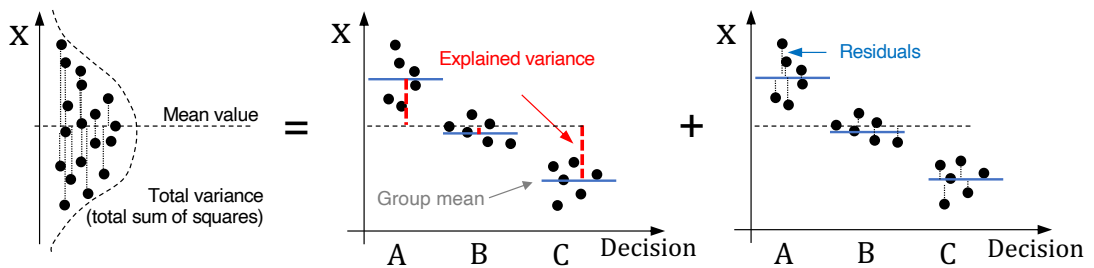


Figure 2. Diagram of the methodology used in this study

188

3.1 Climate clustering

189

190

191

192

193

194

195

196

197

198

199

200

201

We perform a Bayesian clustering to identify climate zones across Chile. To this end, we use the aridity index (PET/P), the p-seasonality, and the fraction of precipitation falling as snow as explanatory variables, since they reflect observed hydrological behaviors (Knoben et al., 2018). PET is computed using the Oudin et al. (2005) formula - available in the R Package airGR (Coron et al., 2017) - which requires air temperature (provided at daily time steps here) and latitude as inputs. To estimate S_n , we consider that snowfall occurs when the mean daily temperature is below 2°C (Jennings et al., 2018; Han et al., 2019; Sepúlveda et al., 2022), and p-seasonality is computed with the formula proposed by Woods (2009).

Prior climate groups are defined with the Autoclass-C software (Cheeseman et al., 1988, 1996), which has been previously used in hydrological applications (e.g., Sawicz et al., 2011). We subsequently refined the clustering results through visual inspection, grouping small clusters based on spatial proximity and climate similarity.

202

3.2 Raw GCM performance

203

204

205

206

207

208

We use the Taylor Skill Score (TSS; Taylor, 2001) to evaluate the role of the raw GCM performance and its interplay with BCM and TS for SDBC-biases and projections at different time scales. The TSS is computed at the grid cell level ($0.05^\circ \times 0.05^\circ$) for the period 1980-2014, contrasting downscaled GCM outputs against the reference dataset, as is commonly done for local climate impact assessments (e.g., Lafon et al., 2013). In this study, TSS is computed for precipitation, as shown in Eq. 1.

209

$$TSS = \frac{4(1 + R)}{(\hat{\sigma} + \frac{1}{\hat{\sigma}})^2 (1 + R_o)} \quad (1)$$

210

211

212

213

214

215

216

217

218

219

where R is the Pearson correlation coefficient between the raw GCM and the reference mean seasonality, and $\hat{\sigma} = \sigma_{GCM}/\sigma_{REF}$ is the ratio between the standard deviation of raw monthly values (σ_{GCM}) and the reference (σ_{REF}). R , and $\hat{\sigma}$ are computed using simulated and observed mean monthly values of each variable (i.e., 12 values of GCMs vs. 12 reference values). R_o is the maximum achievable Pearson correlation coefficient for a specific GCM, which is assumed to be $R_o \cong 1$ to simplify the analysis. When $R \rightarrow R_o$ and $\hat{\sigma} \rightarrow 1$, the $TSS \rightarrow 1$. Alternatively, $TSS \rightarrow 0$ when R decreases or $\hat{\sigma}$ approaches zero or infinity. Hence, TSS ranges between 0 and 1. Further, we compute the TSS for each climate group, estimating the mean group climatology through spatial averages.

220

3.3 Bias correction of GCMs

221

3.3.1 Bias correction methods

222

223

224

225

226

227

228

229

230

231

232

233

234

235

We downscale the raw GCM outputs to the CR2MET grid using inverse distance weighting, considering the four closest GCM grid cells. We use seven bias correction methods, including three univariate and four multivariate techniques, listed in Table 1 and briefly reviewed here. The quantile delta mapping (QDM) preserves the projected change for each quantile while correcting the bias. Empirical cumulative density functions are estimated for the historical reference ($F_{h,ref}$), the raw historical GCM ($F_{h,GCM}$), and the raw projected GCM ($F_{p,GCM}$) to relate (X) with the cumulative probability (τ). For a specific value during the historical period $X_{h,GCM}$, the correction (for pr) is given by $X'_{h,GCM} = F_{h,ref}^{-1}(F_{h,GCM}(X_{h,GCM}))$, while for a projected raw GCM value $X_{p,GCM}$, the corrected value is $X'_{p,GCM} = \Delta \cdot F_{h,GCM}^{-1}(F_{p,GCM}(X_{p,GCM}))$, where Δ is computed as $\Delta = X_{p,GCM}/F_{h,GCM}^{-1}(F_{p,GCM}(X_{p,GCM}))$ for precipitation. The asynchronous regression (AR) relies on a piecewise linear regression calibrated with sorted raw GCM and reference data during a historical period (i.e., $F_{h,ref}$ is a function of $F_{h,GCM}$). Although a simple linear regression could be used, the error in the tails of

236 the regression can be large and, therefore, the data is split by including different knots
 237 (up to six) to reduce errors in low and high values. To bias-correct projected values, the
 238 calibrated piecewise linear regression is applied. The quantile regressions neural network
 239 (QRNN) uses neural networks to bias correct the sorted data (i.e., quantiles) from sim-
 240 ulations and the reference. QRNN is a flexible model since it does not assume a specific
 241 relationship between the raw GCM and the reference data.
 242 The rank resampling for distributions and dependences (R^2D^2) corrects the covariance
 243 among sites and/or variables through four steps: (i) the univariate bias correction of each
 244 variable/site separately, (ii) the selection of one variable/site and the computation of the
 245 ranking for all variables/sites, (iii) for a specific date, select the same ranking in the ref-
 246 erence period for the dimension selected, and (iv) the shuffling of the other variables/sites
 247 to maintain rank structure.
 248 The ‘multivariate bias correction’ family (MBC) includes three different methods using
 249 the Pearson correlation coefficient (MBCp), the Spearman rank correlation coefficient
 250 (MBCr), and an N-dimensional probability density function (MBCn) to transform the
 251 raw correlated GCM data (i.e., the intervariable dependence structure) through consec-
 252 utive iterations. For MBCp and MBCr, the transformation relies on the Cholesky ma-
 253 trix decomposition and the correction of the covariance matrix. Conversely, MBCn re-
 254 lies on an orthogonal rotation, the application of QDM to these orthogonal variables, and,
 255 finally, the application of an inverse matrix (the one used to compute the orthogonal vari-
 256 ables) to obtain the resulting data. The reader is referred to the studies listed in Table
 257 1 for more details on the methods.

Table 1. Methods considered in this study to bias-correct GCMs outputs (pr, tmax, and tmin).

Acronym	Name	Type	Reference
QDM	Quantile Delta Mapping		Cannon et al. (2015)
AR	Asynchronous Regression	Univariate	Dettinger et al. (2004); Stoner et al. (2013)
QRNN	Quantile Regression Neural Network		Cannon (2011)
R^2D^2	Rank Resampling for Distributions and Dependences		Vrac and Thao (2020)
MBCp	Multivariate Bias Correction method - Pearson	Multivariate	Cannon (2016)
MBCr	Multivariate Bias Correction method - Rank		
MBCn	Multivariate Bias Correction method - QDM		Cannon (2018)

258 We stress that it is not our aim to perform detailed comparisons among different
 259 bias correction techniques but to quantify the impact of this and other methodological
 260 choices on historical biases and projected changes in climate indices. All bias correction
 261 methods were applied using the statistical software ‘R’ (<http://www.r-project.org/>). The
 262 QDM, MBCp, MBCr, MBCn, and R^2D^2 methods were applied using the library ‘MBC’
 263 (Cannon, 2018). QRNN was implemented using the ‘qrnn’ library (also available in R),
 264 while the AR method was implemented following Stoner et al. (2013). To reduce the com-
 265 putational effort, we randomly select 100 grid cells within each climate group, and all
 266 subsequent analyses are conducted at these grid cells ($100 \cdot N_{clusters}$).

267 3.3.2 Choice of the temporal stratification

268 Bias correction methods can be applied using different stratification strategies. For
 269 example, a BCM can be applied at daily time steps using all the data in the historical
 270 period (usually 30 years), which means that all $\sim 10,950$ days (~ 365 days \cdot 30 years) are
 271 simultaneously bias-corrected. For a seasonal TS, BCMs are applied four times, each one
 272 considering ~ 2730 days (~ 91 days \cdot 30 years), whereas for a monthly TS, the BCM is
 273 applied 12 times considering ~ 900 days (~ 30 days \cdot 30 years). Note that other tempo-

274 ral stratifications could be considered. Here, we applied BCMs to daily time series of pr,
 275 tmax, and tmin (e.g., Rastogi et al., 2022) using the entire time series in the historical
 276 period (1980-2014), and stratifying the data seasonally and monthly, since these TSs are
 277 typically considered for climate change impact assessments. For all combinations of BCM
 278 and TS, we obtained daily time series from 1980 to 2100.

279 3.4 Climate indices

280 We consider several climate indices that are relevant to reproduce historically ob-
 281 served hydrological responses (e.g., Gutmann et al., 2014), including (i) mean annual,
 282 seasonal, and monthly total precipitation, (ii) highest 1% daily precipitation, (iii), wet-
 283 day fraction, (iv) wet and dry-spell lengths, (v) fraction of precipitation falling as snow,
 284 and (vi) annual, seasonal and monthly averages of mean daily temperature and diurnal
 285 temperature ranges. To estimate the mean annual snowfall, we add all precipitation amounts
 286 for days with a mean daily temperature below 2°C. Wet-spell and dry-spell lengths (mean
 287 consecutive rainy and non-rainy days, respectively), as well as the wet-day fraction (mean
 288 fraction of rainy days) are computed as in Gutmann et al. (2014), considering 0.1 mm/d
 289 as a threshold. To examine the capability of BCMs to replicate historically observed cli-
 290 mate indices, we computed the difference between SDBC-GCM outputs and the refer-
 291 ence dataset during the historical period 1980-2014 as a percent bias (hereafter referred
 292 to as biases). Additionally, we analyze the effects of BCMs on climate projections by com-
 293 puting the relative change for the period 2065-2099 with respect to the historical period
 294 (1980-2014).

295 3.5 Analysis of Variance

296 To evaluate the relative contribution of the BCM and TS decisions to the spread
 297 of SDBC-biases we perform, for each combination of GCM and grid cell, an analysis of
 298 variance (ANOVA). In this case, the ANOVA is simplified as:

$$299 \quad TV = BCM + AP + Residual \quad (2)$$

300 where TV stands for the total variance of SDBC-biases, and the residual term is the vari-
 301 ance not explained by the BCM nor the TS for a specific GCM-grid cell combination.
 302 If the choice of TS had no impact on the biases in climate indices. In that case, the ap-
 303 plication of Supposey BCM should be able to reduce biases at all temporal scales (e.g.,
 304 annual, seasonal, or monthly), regardless of the GCM considered. To summarize the in-
 305 formation at the grid cell level, we compute the average of BCM/TV , TS/TV , and $Residual/TV$
 306 fractions across GCMs, whereas for the climate groups, we compute the mean relative
 307 contribution (estimated by BCM/TV , TS/TV and $Residual/TV$) of TS and BCM to
 308 the spread as the average of fractions across the grid cells within that group.

309 4 Results

310 We show the climate clustering results, the historical biases after applying the BCMs,
 311 and the relative contributions of different methodological choices to historical biases of
 312 climate indices at the annual and seasonal scales. Further, we include the TSS perfor-
 313 mance to examine connections between the raw seasonality of the GCMs and the selec-
 314 tion of BCM and TS. For simplicity, we only show the results for precipitation, and the
 315 remaining variables can be found in the Supporting Information.

316 4.1 Clustering

317 The Bayesian clustering and subsequent spatial aggregation through visual inspec-
 318 tion provided ten climate groups for continental Chile (Figure 3). In general, the clus-
 319 ters follow two main climate patterns in Chile: (i) a latitudinal precipitation gradient,

320 from very arid (north) to humid (south), and (ii) a west-east gradient from the coast to
 321 the Andes Cordillera. Although northern Chile encloses groups 1, 2, and 3, clusters 2
 322 and 3 are located in the Altiplano region, where larger precipitation and lower temper-
 323 atures are observed. Groups 5, 6, and 8 span the coast and valley, whereas groups 4 and
 324 7 are located in the Andes. Finally, groups 9 (the rainiest group) and 10 are in south-
 325 ern Chile, characterized by large precipitation amounts in the Andes Cordillera and the
 326 coast, with decreasing precipitation and temperature towards the east (Patagonia).

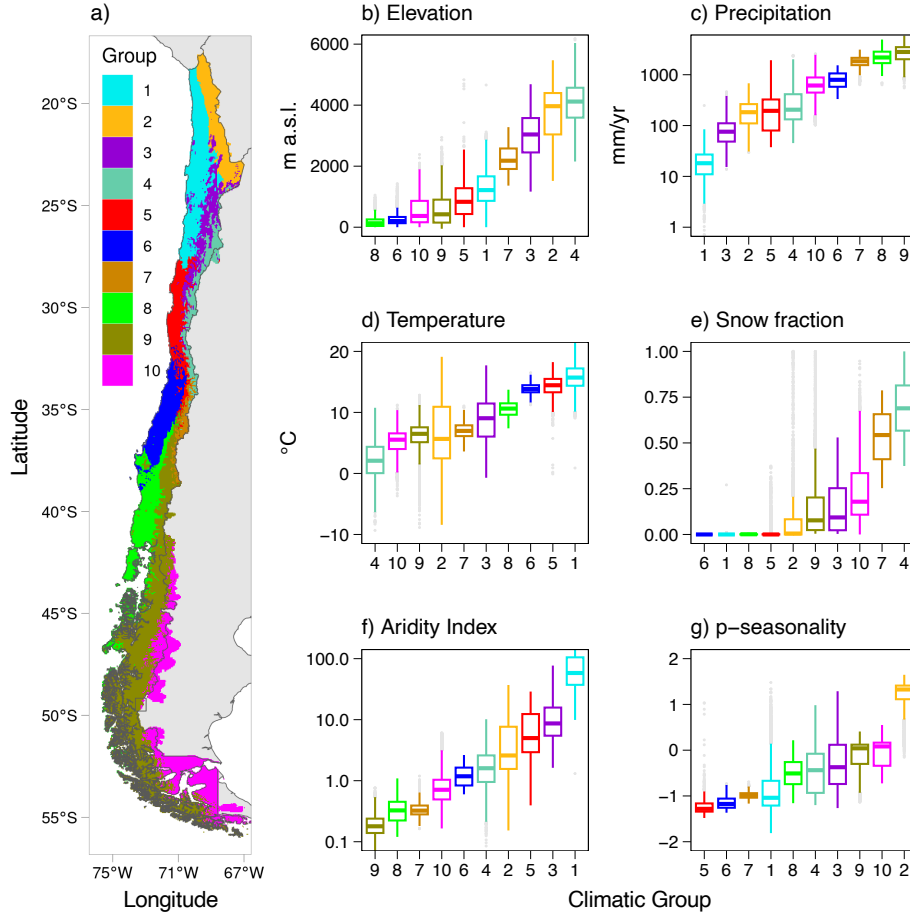


Figure 3. (a) Spatial distribution of climate clusters in continental Chile based on snowfall fraction, aridity index, and p-seasonality. The following attributes are ordered by the median of each group: (b) elevation, (c) precipitation, (d) temperature, (e) snowfall fraction, (f) aridity index, and (g) p-seasonality. All climate indices were computed for the period 1980-2014. Notice that the boxplots in panels b-g are sorted according to the median value, and the group's order on the x-axis differs among variables.

327 4.2 Performance metrics after bias correction

328 Figure 4 shows precipitation biases (after bias correction) in three different climate
 329 groups (the other variables and climate groups can be found in the Supporting Informa-
 330 tion). The results show that, regardless of the combination of GCM, BCM, TS and grid
 331 cell, biases in annual amounts are close to zero (Figure 4a). When the BCM is applied

332 using all the data in the historical period(Figure 4b, left), biases in monthly precipita-
 333 tion amounts can be large, although the magnitude varies among climate groups. In cli-
 334 mate group 2 (Altiplano region), precipitation occurs mostly during the summer (DJF);
 335 in this season, the median bias associated with January precipitation is relatively lower
 336 - though still considerable ($>20\%$) - compared to the remaining months. In group 6, most
 337 precipitation occurs during the winter (JJA), and biases can be found in any month. In
 338 group 10, precipitation falls uniformly throughout the year, with slightly larger amounts
 339 and larger biases during the summer (DJF). When the BCM is applied seasonally (4b,
 340 center), monthly precipitation biases persist. However, these are generally lower com-
 341 pared to the case when the bias correction is applied using the entire dataset, especially
 342 in climate group 10. As expected, biases are nearly removed with a monthly TS (Fig-
 343 ure 4b, right), regardless of the GCM, bias correction method, grid cell, or climate group.

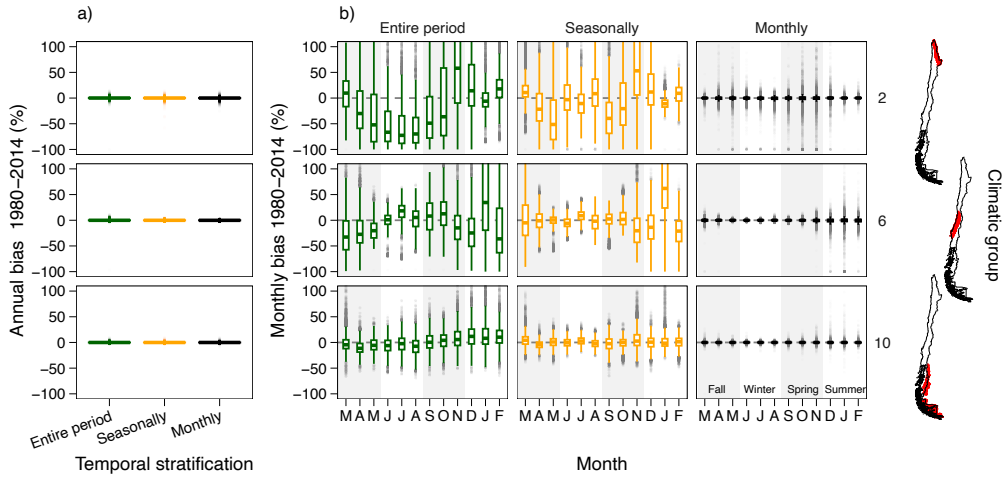


Figure 4. Historical biases in precipitation at the (a) annual and (b) seasonal time scales in three climate groups (rows) after applying the BCMs. The columns in panel b) show results for the three TSs used to apply the BCMs. Each boxplot comprises results from the 100 grid cells within a specific climate group, 29 GCMs, and seven BCMs. The different seasons are highlighted through grey-white areas.

344 Figure 5 displays the relative contributions of the BCM, TS, and residuals for mean
 345 annual, seasonal (summer and winter), and monthly (January and July) precipitation
 346 biases averaged across 1,000 grid cells in continental Chile. We show two seasons and
 347 months to examine possible differences between the dry and wet seasons. Additionally,
 348 the results from different GCMs are stratified according to their historical raw perfor-
 349 mance, measured by the Taylor Skill Score. As in Figure 4, the ANOVA analysis for his-
 350 torical biases shows differences among temporal stratifications, especially when compared
 351 to annual biases (Figure 5a). Because the relative contributions of BCM and TS to pre-
 352 cipitation biases do not greatly differ among climate groups, we show results at the na-
 353 tional scale. The choice of BCM explains most of the variance for the mean annual pre-
 354 cipitation bias, whereas the choice of TS explains almost all the variance for mean sea-
 355 sonal and monthly precipitation biases. It is worth noting that the biases at the annual
 356 scale are, in general, very low (Figure 4, $<1\%$), and that the relative importance of the
 357 choice of TS for seasonal and monthly biases does not decrease for GCMs with high TSS
 358 values. The latter result is counterintuitive since one might expect that GCMs with good
 359 raw precipitation seasonality will be effectively bias-corrected, regardless of the TS se-
 360 lected. For variables related to quantiles (highest 1% daily precipitation, dry and wet-

spell lengths, and wet-day fraction), the relative importance of BCMs increases for GCMs with higher TSS, being BCM the most important decision, even at seasonally and monthly time scales (Figure S1).

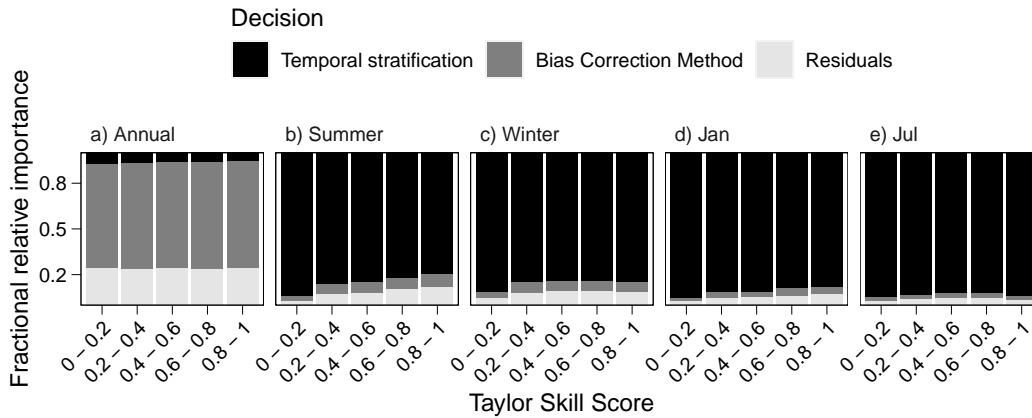


Figure 5. Relative importance (as a fraction averaged from all grid cells and GCMs for continental Chile) of the bias correction method and the temporal stratification to explain the precipitation biases at the annual, seasonal (DJF and JJA), and monthly (January and July) time scales during the historical period (1980-2014), for different levels of historical GCM performance (x-axis). Biases are computed after applying BCMs.

4.3 Projected changes

We now analyze the interplay between the choice of TS, the raw GCM precipitation seasonality, and its effects on projected changes in precipitation for the period 2065-2099 (with respect to 1980-2014) at different time scales. Figure 6 displays projected changes in mean annual, seasonal, and monthly precipitation for one grid cell located in central Chile (red dot in map) and one GCM (INM-CM4-8) with a high R value. For this GCM and grid cell, $TSS = 0.76$ during the period 1980-2014, with a Pearson correlation coefficient between mean monthly raw GCM and reference amounts of 0.98, and a 41% underestimation of the standard deviation. The high value of R indicates a good seasonality of raw GCM outputs. Figure 6 shows that different BCMs yield a high dispersion in projected changes of mean annual precipitation (different lines), with little influence on the selected TS (x-axis of each subplot). Additionally, all BCMs alter the raw GCM projection. For example, if all BCMs are applied using the entire dataset, projected changes in summer precipitation range between -8% to 5%, whereas the raw projection is close to -30%. The application of MBCn using the entire period yields a positive projected change in the mean summer precipitation, while a seasonal and monthly application of the same BCM projects a decrease in summer precipitation. The results for individual months (January and July) reveal more dispersion and interaction among BCMs and the choice of TS. For example, applying the BCM with the entire time series results in positive and negative projections of mean July precipitation (the rainiest month for this grid cell). Similarly, different TSs can also provide different projected signals.

Figure 6 reveals that the choice of TS affects the signal of projected changes in summer precipitation (e.g., for the MBCn method) and, in particular, in January and July precipitation amounts. The TS can be considered relevant for a specific grid cell if it is able to switch the projected signal of a variable for a particular GCM-BCM combination. This is, for example, the case of mean July precipitation (Figure 6), for which the

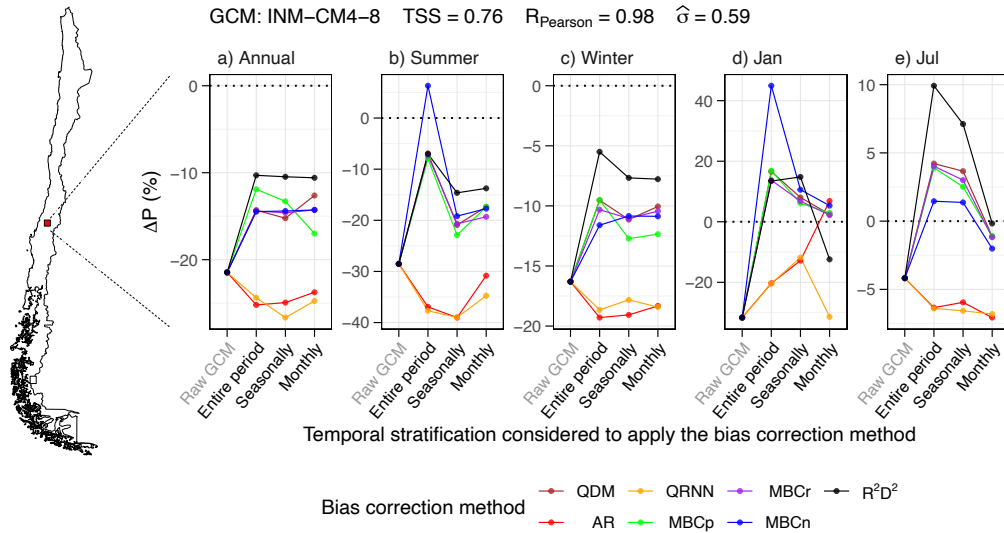


Figure 6. Projected change in annual, seasonal (summer and winter), and monthly (January and July) precipitation for different temporal stratifications (x-axis) and bias correction methods (lines). All combinations of TS and BCM decisions, along with projected changes from the raw (biased) GCMs, are displayed. The results are valid only for the grid cell shown and the GCM INM-CM4-8. The metrics (e.g., TSS) were computed using the raw (biased) GCM data for the period 1980-2014.

390 signal of projected changes is different among TSs for the MBCn, MBCr, and R^2D^2 meth-
 391 ods.

392 Figure 7 shows, for all the grid cells analyzed, the fraction of ‘well-behaved’ GCMs
 393 (i.e., with $TSS \geq 0.7$; e.g., Kwon et al., 2019) for which the selection of TS leads to
 394 different signs in projected precipitation changes. Note that the number of GCMs that
 395 meet the performance requirement - obtained by spatially averaging the number of GCMs
 396 with $TSS \geq 0.7$ at each latitudinal band - varies along the domain. In general, the choice
 397 of TS does not alter the signal of projected changes in mean annual precipitation, although
 398 a few GCMs are affected by this decision in some areas (e.g., northern Chile). Never-
 399 theless, the effects of TS are more evident in seasonal projections (Figure 7b and 7c).
 400 During the summer, >50% of the number of GCMs are affected by the TS in Central
 401 Chile (dry season). During winter, the Altiplano region and part of southern Chile are
 402 largely influenced by the choice of TS. It should be noted, however, that the summer sea-
 403 son in Central Chile and the winter season in the Altiplano region are dry seasons. There-
 404 fore, while the signal of projected changes may vary for different TSs, the precipitation
 405 amounts involved are small. For mean monthly January and July precipitation, the choice
 406 of TS is even more relevant. Indeed, nearly all GCMs are affected by the TS along the
 407 coast of northern Chile, while $\sim 50\%$ of the GCMs yield different signals in projected changes
 408 for different TSs in Central Chile. The case of July is more interesting since it is the raini-
 409 est month in most of continental Chile. In July, $\sim 50\%$ of the GCMs are affected by the
 410 TS along the Central Chilean Andes (western border), impacting the accumulation of
 411 snow and, therefore, meltwater volume and timing estimates for the spring and summer
 412 seasons. In southern Chile, one can find grid cells where GCMs are affected by the TS
 413 decision, though that fraction is lower compared to the Central Chilean Andes.

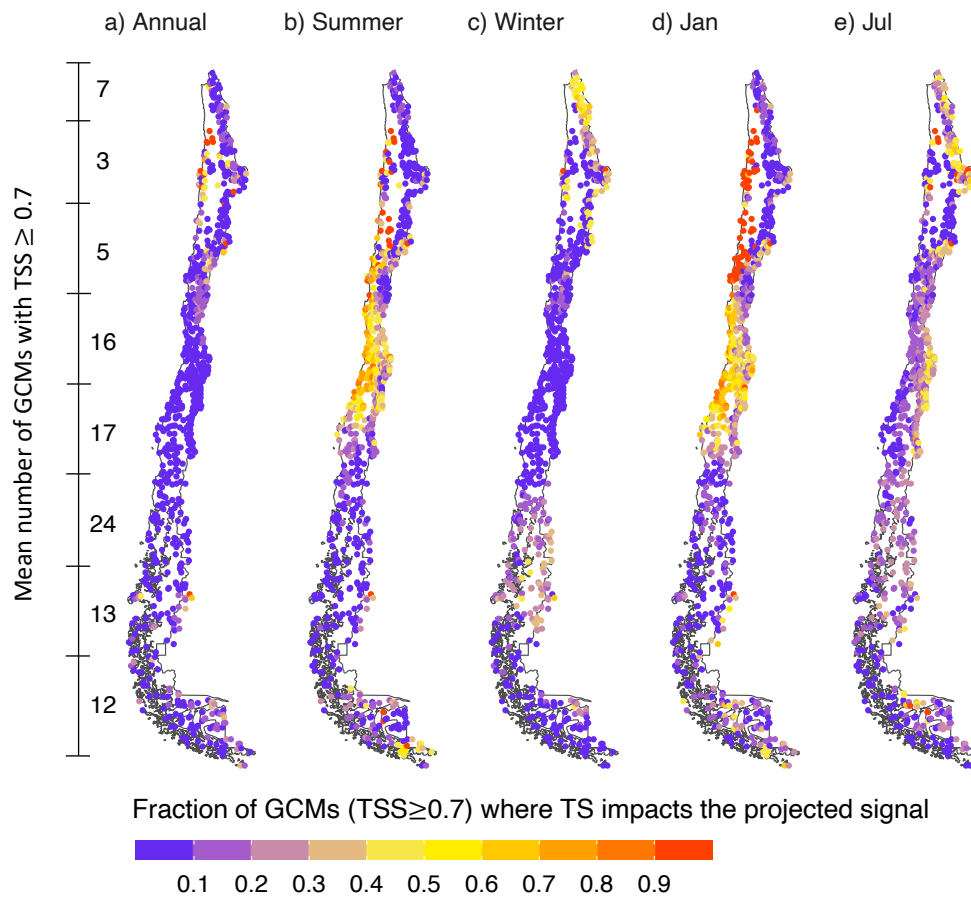


Figure 7. Fraction of GCMs with acceptable performance (i.e., with $TSS \geq 0.7$) for which the TS yields different projected precipitation signals. The number of GCMs that meet the threshold criteria at each $\sim 5^\circ$ latitudinal band is computed as the average of GCMs with $TSS \geq 0.7$ from all grid cells within that band.

414 Figure 8a compares the raw GCM output (obtained from the GCM ACCESS-CM2)
 415 and the reference precipitation seasonality over a historical period at one grid cell located
 416 in central-southern Chile (red dot on the map). For this GCM-grid cell combination, $TSS =$
 417 0.96 , $R = 0.94$ and $\hat{\sigma} = 1.08$. Note that the GCM simulates the maximum monthly
 418 precipitation in July instead of June (when the maximum occurs according to the ref-
 419 erence). Figure 8b displays, for the same GCM-grid cell, the projected precipitation sea-
 420 sonality for each BCM-TS combination (thin lighter lines). The results show that ap-
 421 plying a BCM using the entire period (green lines) provides the same seasonality as the
 422 raw GCM; however, seasonal and monthly TSs distort the raw projected seasonality. Fur-
 423 ther, when BCMS are applied using a monthly TS (black/gray lines), the projected month
 424 of maximum precipitation is June, whereas for seasonal and entire period such month
 425 is July. Additionally, seasonal and monthly TSs yield higher precipitation fractions (com-
 426 pared to the raw GCM) during April and May, and smaller values during September and
 427 October. Such differences in projected precipitation seasonality may affect any subse-
 428 quent analyses of simulated hydrological fluxes and states.

429 To examine the extent to which projected precipitation seasonality is affected by
 430 the temporal stratification, we focus on the projected maximum mean monthly precip-
 431 itation. Hence, we contrast, for each GCM-grid cell combination, three curves obtained
 432 with the three temporal stratifications (each obtained by averaging the projections among
 433 BCMS for each GCM). We consider that the TS affects the projected seasonality if the
 434 month where the maximum mean monthly precipitation amount occurs differs. Conversely,
 435 if such a month is the same for the three TSs, we consider that this decision does not
 436 impact the seasonality. Figure 8c displays the fraction of the number of GCMs with $TSS \geq$
 437 0.7 for which the TS impacts the projected precipitation seasonality. Interestingly, the
 438 number is relatively high ($>40\%$) for most of continental Chile. The fraction of GCMs
 439 affected by the TS decision is even higher in northern Chile, the Central Chilean Andes,
 440 and the Southernmost part of Chile, where more than 60% of GCMs are affected.

441 5 Discussion

442 The results presented here highlight the relevance of the temporal stratification used
 443 when applying bias correction techniques, which affects (i) SDBC-biases in seasonal and
 444 monthly precipitation amounts over a historical period, and (ii) the signal of projected
 445 changes and the seasonality of projections.

446 5.1 Temporal stratification as a source of uncertainty

447 Our results show that the temporal stratification can largely affect precipitation
 448 biases during a historical period, as well as the signal and seasonality of projected changes.
 449 However, this methodological choice has been rarely explored in climate change impact
 450 assessments, and the lack of guidance has motivated the use of more than one TS in some
 451 studies (e.g., Wootten et al., 2021). Further, model errors may not necessarily be removed
 452 in the process. For example, Hakala et al. (2018) obtained that biases in precipitation
 453 and streamflow seasonality remained after applying BCMS. Here, we found that only a
 454 monthly application of the BCM can replicate the reference precipitation seasonality, even
 455 for GCMs with a good raw representation of annual cycles.

456 5.2 Projected seasonality

457 Our study reveals that one of the main effects of selecting different TSs is the possi-
 458 bility to distort the precipitation seasonality projected by raw GCM outputs. In hydro-
 459 logic impact assessments, this artifact may propagate into the timing of simulated
 460 variables like snow accumulation and melting, energy fluxes, and streamflow (Meyer et
 461 al., 2019). Our results show that when the raw GCM seasonality has timing errors (com-

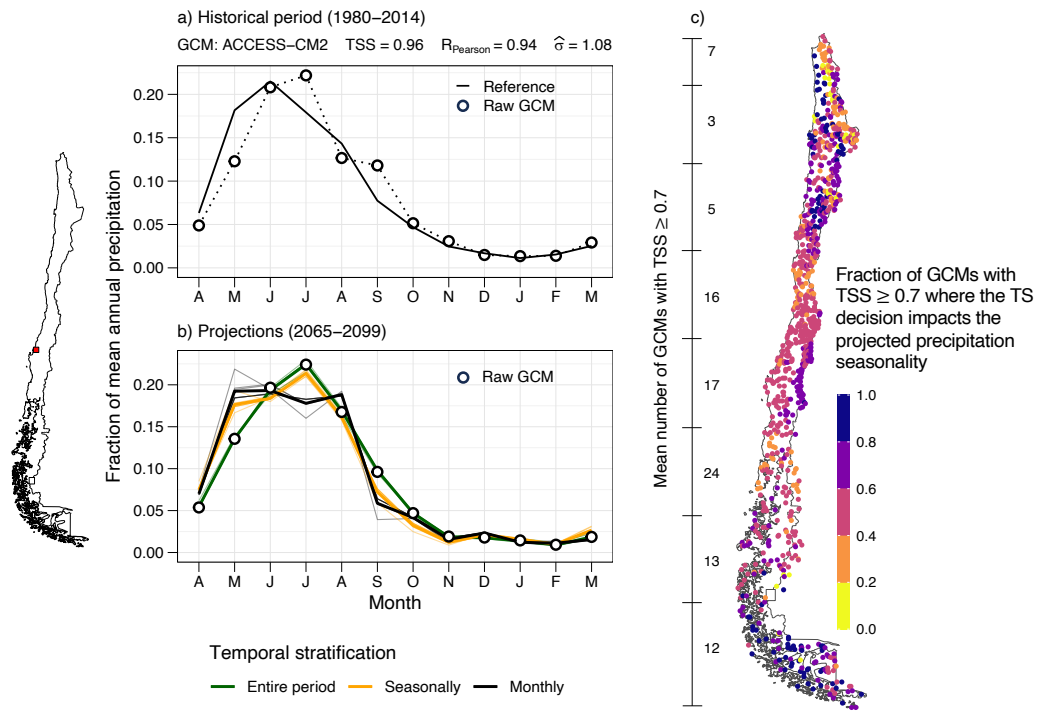


Figure 8. Influence of the temporal stratification used to apply bias correction methods on the projected precipitation seasonality. (a) Dimensionless historical seasonality for one grid cell (red dot on the map) and one GCM (ACCESS-CM2). Note that the sum of monthly fractions is equal to 1. (b) Projected raw (circles) and bias-corrected (colored lines) GCM precipitation seasonality. Lighter and thinner lines represent different BCMs, whereas thick lines represent the average across BCMs. (c) Fraction of the total number GCMs with $TSS \geq 0.7$, for which the temporal stratification yields different projected seasonality, measured as different months for maximum mean monthly precipitation for the 2065-2099 period. In c), the average number of GCMs meeting the TSS criterion is computed for latitudinal bands.

462 pared to the reference), a pronounced shift in the projected seasonality can be obtained
 463 after applying BCs (compared to the case without bias correction). However, when
 464 the raw GCM replicates the historically observed precipitation seasonality reasonably
 465 well, one might expect that different TSs yield the same projected seasonality. To test
 466 this hypothesis, we compare the precipitation seasonality projected with three TSs (bot-
 467 tom panels) by two GCMs (CanESM5 and NorESM2-MM, Figure 9) that replicate an-
 468 nual cycles (i.e., high Pearson correlation coefficients, with GCM and reference maximum
 469 annual mean monthly precipitation being the same, top panels). For GCM CanESM5 (Figure
 470 9a), the choice of TS has little effect on the projected precipitation seasonality. Conversely,
 471 the temporal stratification affects the seasonality projected by NorESM2 (Figure 9b).
 472 For example, if the BCM is applied seasonally and monthly, the months of maximum mean
 473 monthly precipitation are May and August, respectively. Interestingly, $TSS = 0.951$ for
 474 this GCM, which is higher than the value obtained for CanESM5 (0.694), and both GCMs
 475 have similar Pearson correlation coefficients. These results emphasize that even GCMs
 476 with a good raw representation of historical seasonality can be affected by the tempo-
 477 ral stratification used to apply BCs.

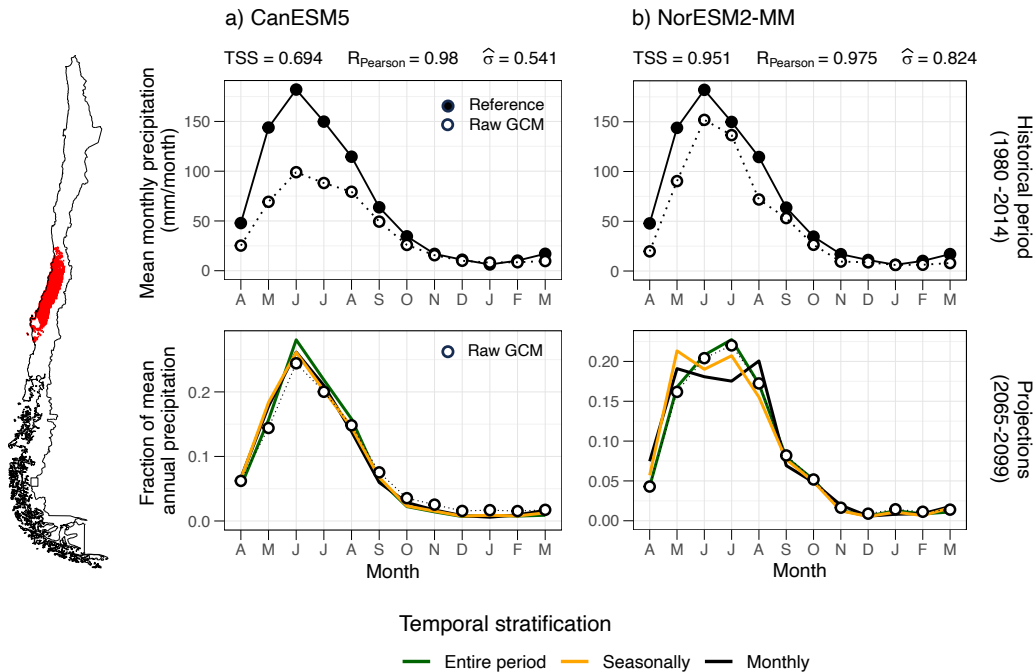


Figure 9. Impact of the temporal stratification used in bias correction for two GCMs. The results presented here are spatially averaged values of the grid cells contained in climate group 6 (highlighted in red on the map). Top row: comparison of the raw GCMs and the reference for the period 1980-2014. Bottom row: projected precipitation seasonality in terms of fraction of mean annual precipitation (average from the seven BCs).

478 5.3 A priori evaluation of the TS impact on projected precipitation sea- 479 sonality

480 Understanding the potential effects of the TS on the projected signal and season-
 481 ality of precipitation from a specific GCM could be helpful for a more detailed assess-

482 ment of climate change and/or hydrological changes. Here, we propose using the linear
 483 scaling method (LSM) (Widmann et al., 2003; Maraun, 2016) - due to its low compu-
 484 tational cost and simplicity (Lafon et al., 2013; Chaubey & Mall, 2023) -, as a quick di-
 485 agnostics tool to inform if the TS may be an influential decision (an example of an LSM
 486 application is provided in Appendix B). The LSM removes the bias from the raw GCM
 487 time series (f_{bias}) through a multiplicative factor for the case of precipitation and an ad-
 488 ditive term for temperature, using an observational dataset as a reference. For exam-
 489 ple, if the reference and raw GCM mean annual precipitation amounts are 500 mm/year
 490 and 650 mm/year, respectively, a factor $f_{bias} = 500/650 = 0.77$ is applied to the raw
 491 GCM time series to remove the bias. Accordingly, seasonal or monthly applications of
 492 LSM require more scaling factors (Maraun et al., 2010). Hence, the raw GCM projected
 493 change (f_{Δ}) is preserved (at the TS time scale), since the scaling factors are typically
 494 considered to be time-invariant. Additionally, the influence of the temporal stratifica-
 495 tion and the reference dataset (in case there is more than one available) can be isolated
 496 for a specific grid cell-GCM combination.

497 Figure 10a illustrates the application of the linear scaling method (dashed lines)
 498 to the GFDL-CM4 GCM in one grid cell (red dot in map), using the entire period and
 499 stratifying the data seasonally and monthly. For this GCM-grid cell combination, $TSS =$
 500 0.72 and $R = 0.7$, and different TSs yield different projected precipitation seasonali-
 501 ties when applying the LSM. Figure 10a shows that the precipitation factors obtained
 502 with LSM agree with the averages obtained from all (seven) bias correction methods (solid
 503 lines).

504 Finally, we examine the capability of the LSM to identify the precipitation season-
 505 ality projected with different TSs correctly. To this end we obtain, for each grid cell-GCM-
 506 TS combination, the precipitation seasonalities from (i) the average between the seven
 507 BCMS, and (ii) the application of the LSM. If the months of the projected maximum pre-
 508 cipitation agree, we consider that the LSM correctly identifies the seasonality, and if this
 509 occurs for the three TSs, we consider that the LSM successfully identifies the projected
 510 bias-corrected seasonality for that specific grid cell-GCM combination. Figure 10a illus-
 511 trates a successful case since, for each TS, the month of maximum precipitation is the
 512 same for the average among seven BCMS and from the LSM. Then we compute, for the
 513 1,000 grid cells analyzed here, the fraction of GCMs for which the LSM successfully iden-
 514 tifies the projected seasonality (accuracy, Figure 10b). The results show that, in almost
 515 all the grid cells, the LSM successfully identifies the projected seasonality of $\sim 70\%$
 516 of the GCMs, whereas for most grid cells ($> 85\%$), the LSM successfully projects the sea-
 517 sonality for more than 85% of the GCMs.

518 **5.4 Limitations and future work**

519 In this study, we selected the SSP5-8.5 scenario and 29 GCMs, although other fu-
 520 ture scenarios and/or a subset of GCMs could be considered to assess the effects on his-
 521 torical biases (after bias correction) and/or future projections. We did not focus on per-
 522 formance metrics for specific GCMs because evaluating the adequacy of particular bias
 523 correction methods is out of the scope of this work; instead, we focus on how these tech-
 524 niques are traditionally applied. Although we selected univariate and multivariate BCMS
 525 (e.g., Q. Guo et al., 2020), quantile-based, neural networks, and linear regressions, dif-
 526 ferent approaches could be considered.

527 Additionally, we did not conduct any hydrological modeling. Instead, we focused
 528 on the repercussions of some decisions on the historical biases and the projected season-
 529 ality of climate variables required to run hydrological and land surface models. However,
 530 previous work has shown that hydrological models tend to amplify biases in the forcings
 531 (Teng et al., 2015). We emphasize that any assessment of climate change impacts should
 532 ensure that the climatological annual cycles of hydrological simulations forced with (i)

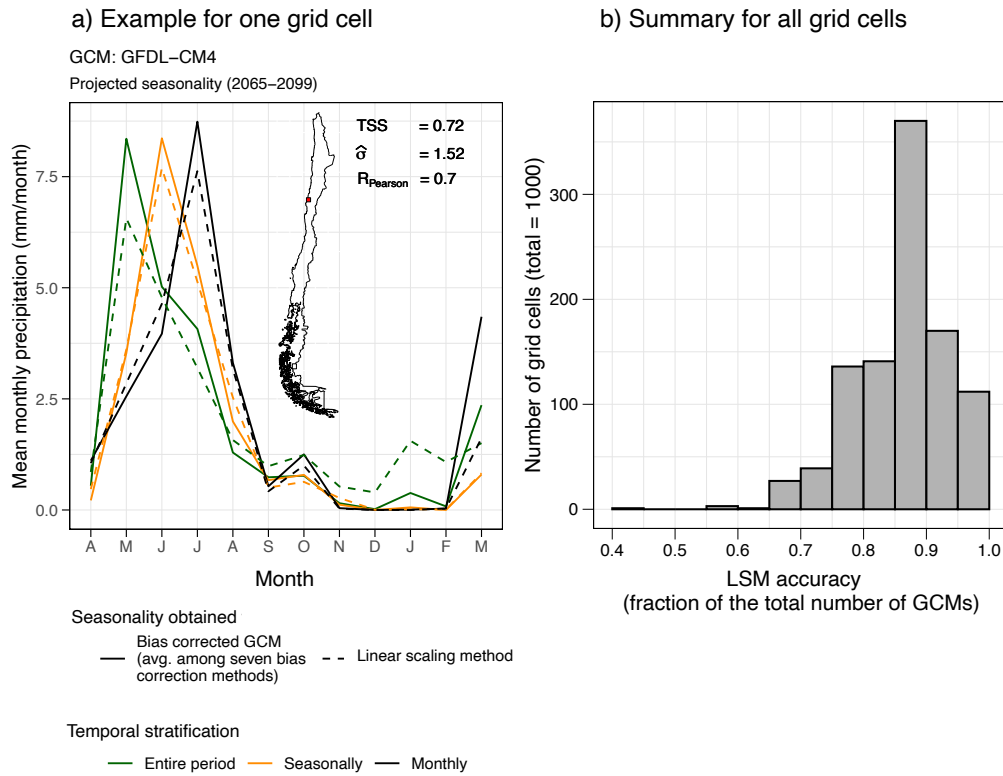


Figure 10. Linear scaling method used as a proxy to estimate the projected precipitation seasonality. (a) Example of projected precipitation seasonalities for one grid cell and one GCM, obtained from applying the LSM and the seven BCMS tested. The metrics summarize the raw (biased) GCM performance for the historical period (1980-2014). (b) LSM accuracy (as a fraction of the total number of GCMs) for all grid cells.

reference data sets and (ii) bias-corrected time series from GCMs/RCMs are similar (Hakala et al., 2018). Hence, verifying the reference and bias-corrected GCM forcing data during a historical period arises as a crucial step (Chen et al., 2013; Clark et al., 2016; Mendoza et al., 2016; Melsen et al., 2019). Future work could consider the impacts of SDBC historical biases and differences in projected seasonality on different aspects of the hydrograph (e.g., mean values, extremes, timing, etc.) and signatures formulated from other variables than streamflow (e.g., SWE, soil moisture; McMillan et al., 2022; Araki et al., 2022).

6 Conclusions

In this paper, we examined how methodological choices involved in GCM bias correction affect historical and future climate portrayals. To this end, we used seven bias correction methods, 29 CMIP6 GCMs, and three temporal stratifications. All the configurations were applied to daily time series of precipitation and maximum and minimum daily temperature derived from the CR2MET gridded observational product, available for continental Chile. Our main findings are as follows:

1. A monthly application of bias correction methods is required to replicate the reference precipitation seasonality, even for GCMs with good raw seasonality.
2. The temporal stratification is the most relevant decision to quantify seasonal and monthly precipitation biases.
3. Different temporal stratifications may yield different projected signals and seasonality, even for GCMs with good raw seasonality.
4. The linear scaling method can be used to estimate the projected seasonality of GCMs and, therefore, to identify the climate models for which the choice of temporal stratification may be critical, before applying more sophisticated and computationally expensive bias correction methods.

Appendix A Selected GCMs

Table A1 shows the GCMs included in this study.

Appendix B Scaling factor example

We illustrate the effects of the temporal stratification by applying the linear scaling method (LSM) (Maraun et al., 2010) for one grid cell-GCM combination. Figure B1a shows monthly precipitation averages from raw GCM outputs, whereas Figure B1b-d shows the bias-corrected GCM values for three different temporal stratifications. Monthly values were obtained from the daily corrected time series. Note that when the entire period is used to bias-correct the GCM, only one factor is applied. In the grid cell analyzed, the reference annual precipitation is 4371 mm, which is below the historical raw GCM amount for the same period (5020 mm). Hence, the raw GCM precipitation time series is multiplied by the factor $f = 4371/5020 = 0.87$, which removes the annual SDBC bias; nevertheless, monthly SDBC-biases persist (see differences between black and blue lines in Figure B1b). When the LSM is applied seasonally, four factors are used to multiply the raw GCM time series. For example, daily values from March, April, and May are bias-corrected by the seasonal factor obtained from the reference (1134 mm/season) and the raw GCM (1498 mm/season) precipitation amounts. In this case, the factor used to bias-correct daily precipitation from March, April, and May is $f_{MAM} = 1134/1498 = 0.76$. Similarly, if the LSM is applied monthly, daily precipitation amounts from March are bias-corrected using the reference (374 mm/month) and raw GCM (498 mm/month), which yields a factor $f = 374/498 = 0.75$. For the monthly TS, the black and blue lines are the same. Note that the projected maximum

Table A1. GCMs considered in this study

GCM	Δlat	Δlon	Institution
ACCESS-CM2	1.25	1.88	Australian Research Council Centre of Excellence for Climate Science, Australia.
ACCESS-ESM1-5	1.25	1.88	
BCC-CSM2-MR	1.11	1.13	Beijing Climate Center, China.
CanESM5	2.77	2.81	Canadian Centre for Climate Modelling and Analysis, Canada.
CMCC-ESM2	0.94	1.25	Euro-Mediterranean Centre on Climate Change Coupled Climate Model, Italy.
CNRM-CM6-1-HR	0.50	0.50	Centre National de Recherches Météorologiques (CNRM), France.
CNRM-CM6-1	1.40	1.40	
CNRM-ESM2-1	1.40	1.41	
E3SM-1-0	1.00	1.00	
EC-Earth3-CC	0.70	0.70	EC-Earth Consortium, Europe.
EC-Earth3-Veg-LR	1.12	1.13	
EC-Earth3-Veg	0.70	0.70	
EC-Earth3	0.70	0.70	
FGOALS-g3	2.18	2.00	Chinese Academy of Sciences Flexible Global Ocean-Atmosphere-Land System Model, China.
GFDL-CM4	1.00	1.25	Geophysical Fluid Dynamics Laboratory, USA.
GFDL-ESM4	1.00	1.25	
INM-CM4-8	1.50	2.00	Institute for Numerical Mathematics, Russia.
INM-CM5-0	1.50	2.00	
IPSL-CM6A-LR	1.27	2.50	Institute Pierre Simon Laplace (IPSL), France.
KACE-1-0-G	1.25	1.88	National Institute of Meteorological Sciences (NIMS) and Korea Meteorological Administration (KMA), South Korea.
KIOST-ESM	1.88	1.88	Korea Institute of Ocean Science and Technology Earth System Model and Its Simulation Characteristics, South Korea.
MIROC-ES2L	2.79	2.81	Japan Agency for Marine-Earth Science and Technology (JAMSTEC), Japan.
MIROC6	1.39	1.41	
MPI-ESM1-2-HR	0.93	0.94	Max Planck Institute for Meteorology (MPI-M), Germany.
MPI-ESM1-2-LR	1.87	1.88	
MRI-ESM2-0	1.11	1.13	Meteorological Research Institute, Japan.
NESM3	1.85	1.88	Nanjing University of Information Science and Technology Earth System Model, China.
NorESM2-MM	0.94	1.25	NorESM Climate modeling Consortium, Oslo, Norway.
TaiESM1	0.94	1.25	Research Center for Environmental Changes, Academia Sinica, Nankang, Taipei, Taiwan.

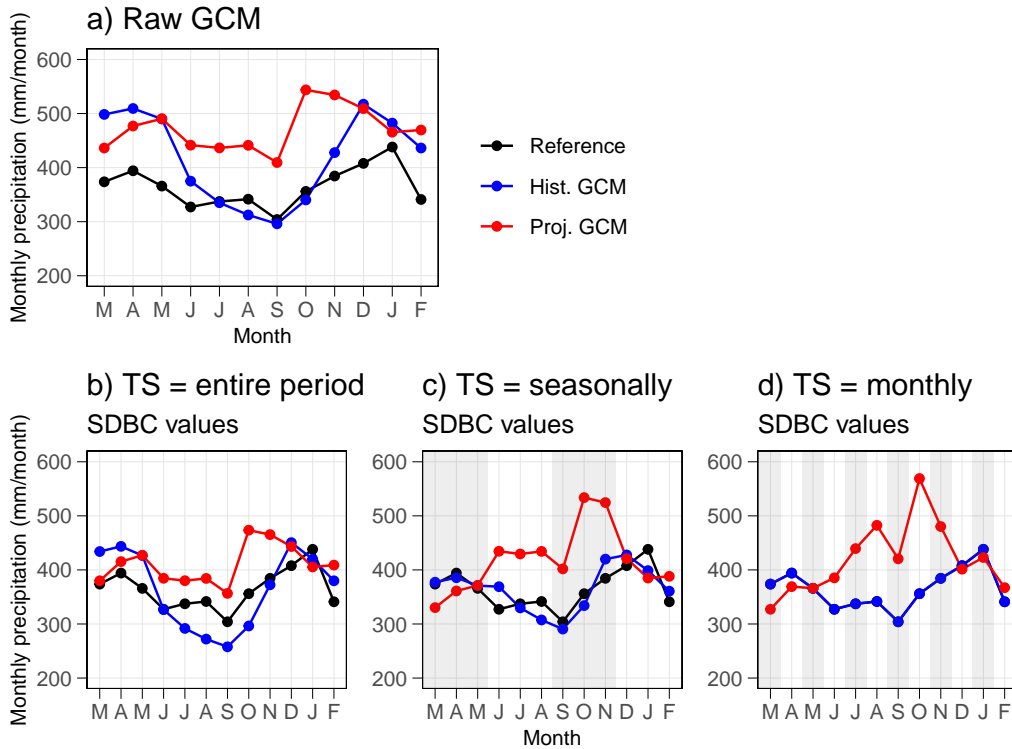


Figure B1. Illustration of the linear scaling method, applied to one grid cell-GCM combination, and its effects on the SDBC-biases and projections. (a) Reference (observational) and raw GCM seasonality during the period 1980-2014 (black and blue lines). The projected raw seasonality is also shown in red (2065-2099). (b), (c) and (d) show the bias-corrected precipitation amounts using the entire period, seasons, and months, respectively, for temporal stratification. The reference value is shown in all panels for completeness, and the shaded areas represent the temporal stratification.

580 monthly precipitation is October for the three TS, which is the same as the raw GCM
 581 projection. However, the projected minimum monthly precipitation is September,
 582 and March for the entire period, season, and monthly application of the LSM, respec-
 583 tively.

584 **Open Research Section**

585 The CR2MET dataset (Boisier et al., 2018) is available at <https://www.cr2.cl/datos-productos-grillados/>. The GCMs data was downloaded from the Earth System Grid Fed-
 586 eration (<https://esgf-node.llnl.gov/search/cmip6/>). All the data used in this study is avail-
 587 able at <https://bhuch.myqnapcloud.com/share.cgi?ssid=43cb3da649cd41ca9bfc42150a855e89>.
 588

589 **Acknowledgments**

590 Nicolás Vásquez and Pablo A. Mendoza received support from the Fondecyt project No.
 591 11200142. Nicolás Vásquez also received support from the Emerging Leaders in the Amer-
 592 icas Program (ELAP) scholarship (Canada) and the ANID Doctorado Nacional schol-

593 arship No. 21230289 (Chile). Pablo A. Mendoza was also supported by ANID/PIA project
594 No. AFB230001.

595 References

- 596 Aceituno, P., Boisier, J. P., Garreaud, R., Rondanelli, R., & Rutllant, J. A. (2021).
597 Climate and Weather in Chile. In *Water resources of chile* (pp. 7–29). doi: 10
598 .1007/978-3-030-56901-3{-}2
- 599 Addor, N., Rössler, O., Köplin, N., Huss, M., Weingartner, R., & Seibert, J.
600 (2014). Robust changes and sources of uncertainty in the projected hy-
601 drological regimes of Swiss catchments. *Water Resources Research*. doi:
602 10.1002/2014WR015549
- 603 Alder, J. R., & Hostetler, S. W. (2019). The Dependence of Hydroclimate Projec-
604 tions in Snow-Dominated Regions of the Western United States on the Choice
605 of Statistically Downscaled Climate Data. *Water Resources Research*. doi:
606 10.1029/2018WR023458
- 607 Araki, R., Branger, F., Wiekenkamp, I., & McMillan, H. (2022, 4). A signature-
608 based approach to quantify soil moisture dynamics under contrasting land-
609 uses. *Hydrological Processes*, 36(4). doi: 10.1002/hyp.14553
- 610 Boisier, J. P., Álvarez-Garretón, C., Cepeda, J., Osses, A., Vásquez, N., & Ron-
611 danelli, R. (2018). CR2MET: A high-resolution precipitation and temperature
612 dataset for hydroclimatic research in Chile. In *Egu general assembly conference*
613 *abstracts* (p. 19739).
- 614 Cannon, A. J. (2011, 9). Quantile regression neural networks: Implementation in
615 R and application to precipitation downscaling. *Computers & Geosciences*,
616 37(9), 1277–1284. doi: 10.1016/j.cageo.2010.07.005
- 617 Cannon, A. J. (2016, 10). Multivariate Bias Correction of Climate Model Output:
618 Matching Marginal Distributions and Intervariable Dependence Structure.
619 *Journal of Climate*, 29(19), 7045–7064. doi: 10.1175/JCLI-D-15-0679.1
- 620 Cannon, A. J. (2018). Multivariate quantile mapping bias correction: an
621 N-dimensional probability density function transform for climate model
622 simulations of multiple variables. *Climate Dynamics*. doi: 10.1007/
623 s00382-017-3580-6
- 624 Cannon, A. J., Sobie, S. R., & Murdock, T. Q. (2015). Bias correction of GCM
625 precipitation by quantile mapping: How well do methods preserve changes in
626 quantiles and extremes? *Journal of Climate*. doi: 10.1175/JCLI-D-14-00754.1
- 627 Chaubey, P. K., & Mall, R. K. (2023, 9). Intensification of Extreme Rainfall in In-
628 dian River Basin: Using Bias Corrected CMIP6 Climate Data. *Earth's Future*,
629 11(9). doi: 10.1029/2023EF003556
- 630 Cheeseman, P., John, R., & Nasa, S. (1996). Bayesian Classification (AutoClass):
631 Theory and Results. *Advances in knowledge discovery and data mining*.
- 632 Cheeseman, P., Kelly, J., Self, M., Stutz, J., Taylor, W., & Freeman, D. (1988, 1).
633 AutoClass: A Bayesian Classification System. *Machine Learning Proceedings*
634 1988, 54–64. doi: 10.1016/B978-0-934613-64-4.50011-6
- 635 Chegwiddden, O. S., Nijssen, B., Rupp, D. E., Arnold, J. R., Clark, M. P., Hamman,
636 J. J., ... Xiao, M. (2019). How Do Modeling Decisions Affect the Spread
637 Among Hydrologic Climate Change Projections? Exploring a Large Ensem-
638 ble of Simulations Across a Diversity of Hydroclimates. *Earth's Future*. doi:
639 10.1029/2018EF001047
- 640 Chen, J., Arsenault, R., Brissette, F. P., & Zhang, S. (2021). Climate Change
641 Impact Studies: Should We Bias Correct Climate Model Outputs or
642 Post-Process Impact Model Outputs? *Water Resources Research*. doi:
643 10.1029/2020WR028638
- 644 Chen, J., Brissette, F. P., Chaumont, D., & Braun, M. (2013, 7). Finding appropri-
645 ate bias correction methods in downscaling precipitation for hydrologic impact

- 646 studies over North America. *Water Resources Research*, 49(7), 4187–4205. doi:
647 10.1002/wrcr.20331
- 648 Clark, M. P., Wilby, R. L., Gutmann, E. D., Vano, J. A., Gangopadhyay, S., Wood,
649 A. W., . . . Brekke, L. D. (2016, 6). Characterizing Uncertainty of the Hy-
650 drologic Impacts of Climate Change. *Current Climate Change Reports*, 2(2),
651 55–64. doi: 10.1007/s40641-016-0034-x
- 652 Coron, L., Thirel, G., Delaigue, O., Perrin, C., & Andréassian, V. (2017, 8). The
653 suite of lumped GR hydrological models in an R package. *Environmental Mod-
654 elling & Software*, 94, 166–171. doi: 10.1016/j.envsoft.2017.05.002
- 655 Dettinger, Cayan, D., Meyer, M., & Jeton, A. (2004). Simulated Hydrologic Re-
656 sponses To Climate Variations. *Climatic Change*.
- 657 DGA. (2022). *Homologación del cálculo hidrológico para la estimación de la oferta
658 natural del agua histórica y futura en Chile*. (Tech. Rep.). SIT N° 524. Min-
659 isterio de Obras Públicas, Dirección General de Aguas, División de Estudios
660 y Planificación, Chile. Elaborado por Universidad de Chile, Facultad de Cien-
661 cias Físicas y Matemáticas. Retrieved from [https://snia.mop.gob.cl/
662 repositoriodga/handle/20.500.13000/126394](https://snia.mop.gob.cl/repositoriodga/handle/20.500.13000/126394)
- 663 Di Virgilio, G., Ji, F., Tam, E., Nishant, N., Evans, J. P., Thomas, C., . . . Delage,
664 F. (2022, 4). Selecting CMIP6 GCMs for CORDEX Dynamical Downscal-
665 ing: Model Performance, Independence, and Climate Change Signals. *Earth's
666 Future*, 10(4). doi: 10.1029/2021EF002625
- 667 François, B., Vrac, M., Cannon, A. J., Robin, Y., & Allard, D. (2020, 6). Multi-
668 variate bias corrections of climate simulations: which benefits for which losses?
669 *Earth System Dynamics*, 11(2), 537–562. doi: 10.5194/esd-11-537-2020
- 670 Ghimire, U., Srinivasan, G., & Agarwal, A. (2019, 3). Assessment of rainfall bias
671 correction techniques for improved hydrological simulation. *International Jour-
672 nal of Climatology*, 39(4), 2386–2399. doi: 10.1002/joc.5959
- 673 Guo, J., Wang, X., Fan, Y., Liang, X., Jia, H., & Liu, L. (2023, 4). How Ex-
674 treme Events in China Would Be Affected by Global Warming—Insights
675 From a Bias-Corrected CMIP6 Ensemble. *Earth's Future*, 11(4). doi:
676 10.1029/2022EF003347
- 677 Guo, Q., Chen, J., Zhang, X. J., Xu, C., & Chen, H. (2020, 5). Impacts of Us-
678 ing State-of-the-Art Multivariate Bias Correction Methods on Hydrologi-
679 cal Modeling Over North America. *Water Resources Research*, 56(5). doi:
680 10.1029/2019WR026659
- 681 Gutiérrez, J. M., Maraun, D., Widmann, M., Huth, R., Hertig, E., Benestad, R.,
682 . . . Pagé, C. (2019, 7). An intercomparison of a large ensemble of statistical
683 downscaling methods over Europe: Results from the VALUE perfect predic-
684 tor cross-validation experiment. *International Journal of Climatology*, 39(9),
685 3750–3785. doi: 10.1002/joc.5462
- 686 Gutmann, E., Pruitt, T., Clark, M. P., Brekke, L., Arnold, J. R., Raff, D. A., &
687 Rasmussen, R. M. (2014). An intercomparison of statistical downscaling meth-
688 ods used for water resource assessments in the United States. *Water Resources
689 Research*. doi: 10.1002/2014WR015559
- 690 Haerter, J. O., Hagemann, S., Moseley, C., & Piani, C. (2011, 3). Climate model
691 bias correction and the role of timescales. *Hydrology and Earth System Sci-
692 ences*, 15(3), 1065–1079. doi: 10.5194/hess-15-1065-2011
- 693 Hagemann, S., Chen, C., Haerter, J. O., Heinke, J., Gerten, D., & Piani, C. (2011,
694 8). Impact of a Statistical Bias Correction on the Projected Hydrological
695 Changes Obtained from Three GCMs and Two Hydrology Models. *Journal of
696 Hydrometeorology*, 12(4), 556–578. doi: 10.1175/2011JHM1336.1
- 697 Hakala, K., Addor, N., & Seibert, J. (2018, 8). Hydrological Modeling to Evaluate
698 Climate Model Simulations and Their Bias Correction. *Journal of Hydrometeo-
699 rology*, 19(8), 1321–1337. doi: 10.1175/JHM-D-17-0189.1
- 700 Han, P., Long, D., Han, Z., Du, M., Dai, L., & Hao, X. (2019, 4). Improved un-

- 701 understanding of snowmelt runoff from the headwaters of China's Yangtze River
 702 using remotely sensed snow products and hydrological modeling. *Remote*
 703 *Sensing of Environment*, 22(4), 44–59. doi: 10.1016/j.rse.2019.01.041
- 704 Hanus, S., Hrachowitz, M., Zekollari, H., Schoups, G., Vizcaino, M., & Kaitna, R.
 705 (2021). Future changes in annual, seasonal and monthly runoff signatures
 706 in contrasting Alpine catchments in Austria. *Hydrology and Earth System*
 707 *Sciences*. doi: 10.5194/hess-25-3429-2021
- 708 Hattermann, F. F., Vetter, T., Breuer, L., Su, B., Daggupati, P., Donnelly, C., ...
 709 Krysnova, V. (2018). Sources of uncertainty in hydrological climate im-
 710 pact assessment: A cross-scale study. *Environmental Research Letters*. doi:
 711 10.1088/1748-9326/aa9938
- 712 Her, Y., Yoo, S. H., Cho, J., Hwang, S., Jeong, J., & Seong, C. (2019). Uncertainty
 713 in hydrological analysis of climate change: multi-parameter vs. multi-GCM
 714 ensemble predictions. *Scientific Reports*. doi: 10.1038/s41598-019-41334-7
- 715 Hersbach, H., Bell, B., Berrisford, P., Hirahara, S., Horányi, A., Muñoz-Sabater, J.,
 716 ... Thépaut, J. (2020, 7). The ERA5 global reanalysis. *Quarterly Journal of*
 717 *the Royal Meteorological Society*, 146(730), 1999–2049. doi: 10.1002/qj.3803
- 718 Hess, P., Lange, S., Schötz, C., & Boers, N. (2023, 10). Deep Learning for Bias-
 719 Correcting CMIP6-Class Earth System Models. *Earth's Future*, 11(10). doi:
 720 10.1029/2023EF004002
- 721 Jennings, K. S., Winchell, T. S., Livneh, B., & Molotch, N. P. (2018, 3). Spatial
 722 variation of the rain–snow temperature threshold across the Northern Hemi-
 723 sphere. *Nature Communications*, 9(1), 1148. doi: 10.1038/s41467-018-03629-7
- 724 Knoben, W. J., Woods, R. A., & Freer, J. E. (2018). A Quantitative Hydrologi-
 725 cal Climate Classification Evaluated With Independent Streamflow Data. *Wa-*
 726 *ter Resources Research*. doi: 10.1029/2018WR022913
- 727 Kwon, S., Kim, J., Boo, K., Shim, S., Kim, Y., & Byun, Y. (2019, 3). Performance-
 728 based projection of the climate-change effects on precipitation extremes in
 729 East Asia using two metrics. *International Journal of Climatology*, 39(4),
 730 2324–2335. doi: 10.1002/joc.5954
- 731 Lafon, T., Dadson, S., Buys, G., & Prudhomme, C. (2013, 5). Bias correction
 732 of daily precipitation simulated by a regional climate model: a comparison
 733 of methods. *International Journal of Climatology*, 33(6), 1367–1381. doi:
 734 10.1002/joc.3518
- 735 Maraun, D. (2016, 12). Bias Correcting Climate Change Simulations - a Critical Re-
 736 view. *Current Climate Change Reports*, 2(4), 211–220. doi: 10.1007/s40641-
 737 -016-0050-x
- 738 Maraun, D., Wetterhall, F., Ireson, A. M., Chandler, R. E., Kendon, E. J., Wid-
 739 mann, M., ... Thiele-Eich, I. (2010, 9). Precipitation downscaling under
 740 climate change: Recent developments to bridge the gap between dynami-
 741 cal models and the end user. *Reviews of Geophysics*, 48(3), RG3003. doi:
 742 10.1029/2009RG000314
- 743 Matiu, M., & Hanzer, F. (2022, 6). Bias adjustment and downscaling of snow cover
 744 fraction projections from regional climate models using remote sensing for the
 745 European Alps. *Hydrology and Earth System Sciences*, 26(12), 3037–3054. doi:
 746 10.5194/hess-26-3037-2022
- 747 Maurer, E. P., & Pierce, D. W. (2014, 3). Bias correction can modify climate
 748 model simulated precipitation changes without adverse effect on the en-
 749 semble mean. *Hydrology and Earth System Sciences*, 18(3), 915–925. doi:
 750 10.5194/hess-18-915-2014
- 751 McMillan, H. K., Gnann, S. J., & Araki, R. (2022, 6). Large Scale Evaluation of Re-
 752 lationships Between Hydrologic Signatures and Processes. *Water Resources Re-*
 753 *search*, 58(6). doi: 10.1029/2021WR031751
- 754 Melsen, L. A., Addor, N., Mizukami, N., Newman, A. J., Torfs, P. J., Clark, M. P.,
 755 ... Teuling, A. J. (2018). Mapping (dis)agreement in hydrologic projections.

- 756 *Hydrology and Earth System Sciences*. doi: 10.5194/hess-22-1775-2018
- 757 Melsen, L. A., Teuling, A. J., Torfs, P. J., Zappa, M., Mizukami, N., Mendoza,
- 758 P. A., . . . Uijlenhoet, R. (2019, 1). Subjective modeling decisions can sig-
- 759 nificantly impact the simulation of flood and drought events. *Journal of*
- 760 *Hydrology*, 568, 1093–1104. doi: 10.1016/J.JHYDROL.2018.11.046
- 761 Mendoza, P. A., Clark, M. P., Mizukami, N., Gutmann, E. D., Arnold, J. R.,
- 762 Brekke, L. D., & Rajagopalan, B. (2016). How do hydrologic modeling deci-
- 763 sions affect the portrayal of climate change impacts? *Hydrological Processes*.
- 764 doi: 10.1002/hyp.10684
- 765 Meyer, J., Kohn, I., Stahl, K., Hakala, K., Seibert, J., & Cannon, A. J. (2019, 3).
- 766 Effects of univariate and multivariate bias correction on hydrological impact
- 767 projections in alpine catchments. *Hydrology and Earth System Sciences*, 23(3),
- 768 1339–1354. doi: 10.5194/hess-23-1339-2019
- 769 O'Neill, B. C., Tebaldi, C., van Vuuren, D. P., Eyring, V., Friedlingstein, P., Hurtt,
- 770 G., . . . Sanderson, B. M. (2016, 9). The Scenario Model Intercomparison
- 771 Project (ScenarioMIP) for CMIP6. *Geoscientific Model Development*, 9(9),
- 772 3461–3482. doi: 10.5194/gmd-9-3461-2016
- 773 Oudin, L., Hervieu, F., Michel, C., Perrin, C., Andréassian, V., Anctil, F., &
- 774 Loumagne, C. (2005, 3). Which potential evapotranspiration input for a
- 775 lumped rainfall–runoff model? *Journal of Hydrology*, 303(1-4), 290–306. doi:
- 776 10.1016/j.jhydrol.2004.08.026
- 777 Pierce, D. W., Cayan, D. R., Maurer, E. P., Abatzoglou, J. T., & Hegewisch, K. C.
- 778 (2015, 12). Improved Bias Correction Techniques for Hydrological Simulations
- 779 of Climate Change*. *Journal of Hydrometeorology*, 16(6), 2421–2442. doi:
- 780 10.1175/JHM-D-14-0236.1
- 781 Rastogi, D., Kao, S., & Ashfaq, M. (2022, 8). How May the Choice of Downscaling
- 782 Techniques and Meteorological Reference Observations Affect Future Hydrocli-
- 783 mate Projections? *Earth's Future*, 10(8). doi: 10.1029/2022EF002734
- 784 Reiter, P., Gutjahr, O., Schefczyk, L., Heinemann, G., & Casper, M. (2018, 3). Does
- 785 applying quantile mapping to subsamples improve the bias correction of daily
- 786 precipitation? *International Journal of Climatology*, 38(4), 1623–1633. doi:
- 787 10.1002/joc.5283
- 788 Ruffault, J., Martin-StPaul, N. K., Duffet, C., Goge, F., & Mouillot, F. (2014, 7).
- 789 Projecting future drought in Mediterranean forests: bias correction of climate
- 790 models matters! *Theoretical and Applied Climatology*, 117(1-2), 113–122. doi:
- 791 10.1007/s00704-013-0992-z
- 792 Sawicz, K., Wagener, T., Sivapalan, M., Troch, P. A., & Carrillo, G. (2011). Catch-
- 793 ment classification: empirical analysis of hydrologic similarity based on catch-
- 794 ment function in the eastern USA. *Hydrology and Earth System Sciences*
- 795 *Discussions*. doi: 10.5194/hessd-8-4495-2011
- 796 Sepúlveda, U. M., Mendoza, P. A., Mizukami, N., & Newman, A. J. (2022, 7).
- 797 Revisiting parameter sensitivities in the variable infiltration capacity model
- 798 across a hydroclimatic gradient. *Hydrology and Earth System Sciences*, 26(13),
- 799 3419–3445. doi: 10.5194/hess-26-3419-2022
- 800 Stoner, A. M., Hayhoe, K., Yang, X., & Wuebbles, D. J. (2013). An asynchronous
- 801 regional regression model for statistical downscaling of daily climate variables.
- 802 *International Journal of Climatology*. doi: 10.1002/joc.3603
- 803 Switanek, M. B., Troch, P. A., Castro, C. L., Leuprecht, A., Chang, H.-I., Mukher-
- 804 jee, R., & Demaria, E. M. C. (2017, 6). Scaled distribution mapping:
- 805 a bias correction method that preserves raw climate model projected
- 806 changes. *Hydrology and Earth System Sciences*, 21(6), 2649–2666. doi:
- 807 10.5194/hess-21-2649-2017
- 808 Taylor, K. E. (2001, 4). Summarizing multiple aspects of model performance in
- 809 a single diagram. *Journal of Geophysical Research: Atmospheres*, 106(D7),
- 810 7183–7192. doi: 10.1029/2000JD900719

- 811 Teng, J., Potter, N. J., Chiew, F. H. S., Zhang, L., Wang, B., Vaze, J., & Evans,
812 J. P. (2015, 2). How does bias correction of regional climate model precipi-
813 tation affect modelled runoff? *Hydrology and Earth System Sciences*, *19*(2),
814 711–728. doi: 10.5194/hess-19-711-2015
- 815 Teutschbein, C., & Seibert, J. (2010, 7). Regional Climate Models for Hy-
816 drological Impact Studies at the Catchment Scale: A Review of Recent
817 Modeling Strategies. *Geography Compass*, *4*(7), 834–860. doi: 10.1111/
818 j.1749-8198.2010.00357.x
- 819 Vano, J. A., Kim, J. B., Rupp, D. E., & Mote, P. W. (2015). Selecting climate
820 change scenarios using impact-relevant sensitivities. *Geophysical Research Let-
821 ters*. doi: 10.1002/2015GL063208
- 822 Vásquez, N., Cepeda, J., Gómez, T., Mendoza, P. A., Lagos, M., Boisier, J. P.,
823 ... Vargas, X. (2021). Catchment-Scale Natural Water Balance in Chile.
824 In (pp. 189–208). Retrieved from [http://link.springer.com/10.1007/
825 978-3-030-56901-3_9](http://link.springer.com/10.1007/978-3-030-56901-3_9) doi: 10.1007/978-3-030-56901-3{_}9
- 826 Vicuña, S., Vargas, X., Boisier, J. P., Mendoza, P. A., Gómez, T., Vásquez, N., &
827 Cepeda, J. (2021). Impacts of Climate Change on Water Resources in Chile.
828 In B. Fernández & J. Gironás (Eds.), *Water resources of chile* (pp. 347–363).
829 Cham: Springer International Publishing. Retrieved from [https://doi.org/
830 10.1007/978-3-030-56901-3_19](https://doi.org/10.1007/978-3-030-56901-3_19) doi: 10.1007/978-3-030-56901-3{_}19
- 831 Vogel, E., Johnson, F., Marshall, L., Bende-Michl, U., Wilson, L., Peter, J. R.,
832 ... Duong, V. C. (2023, 7). An evaluation framework for downscaling and
833 bias correction in climate change impact studies. *Journal of Hydrology*, *622*,
834 129693. doi: 10.1016/j.jhydrol.2023.129693
- 835 Vrac, M., & Thao, S. (2020, 11). R2D2; v2.0: accounting for temporal dependences
836 in multivariate bias correction via analogue rank resampling. *Geoscientific
837 Model Development*, *13*(11), 5367–5387. doi: 10.5194/gmd-13-5367-2020
- 838 Wan, Z. (2014, 1). New refinements and validation of the collection-6 MODIS land-
839 surface temperature/emissivity product. *Remote Sensing of Environment*, *140*,
840 36–45. doi: 10.1016/j.rse.2013.08.027
- 841 Werner, A. T., & Cannon, A. J. (2016, 4). Hydrologic extremes – an intercompar-
842 ison of multiple gridded statistical downscaling methods. *Hydrology and Earth
843 System Sciences*, *20*(4), 1483–1508. doi: 10.5194/hess-20-1483-2016
- 844 Widmann, M., Bretherton, C. S., & Salathé, E. P. (2003, 3). Statistical Precipi-
845 tation Downscaling over the Northwestern United States Using Numerically
846 Simulated Precipitation as a Predictor*. *Journal of Climate*, *16*(5), 799–816.
847 doi: 10.1175/1520-0442(2003)016(0799:SPDOTN)2.0.CO;2
- 848 Wilby, R. L., & Dessai, S. (2010). Robust adaptation to climate change. *Weather*.
849 doi: 10.1002/wea.543
- 850 Woods, R. A. (2009, 10). Analytical model of seasonal climate impacts on snow hy-
851 drology: Continuous snowpacks. *Advances in Water Resources*, *32*(10), 1465–
852 1481. doi: 10.1016/j.advwatres.2009.06.011
- 853 Wootten, A. M., Dixon, K. W., Adams-Smith, D. J., & McPherson, R. A. (2021,
854 2). Statistically downscaled precipitation sensitivity to gridded observation
855 data and downscaling technique. *International Journal of Climatology*, *41*(2),
856 980–1001. doi: 10.1002/joc.6716
- 857 Wu, Y., Miao, C., Fan, X., Gou, J., Zhang, Q., & Zheng, H. (2022, 11). Quanti-
858 fying the Uncertainty Sources of Future Climate Projections and Narrowing
859 Uncertainties With Bias Correction Techniques. *Earth's Future*, *10*(11). doi:
860 10.1029/2022EF002963
- 861 Xavier, A. C. F., Martins, L. L., Rudke, A. P., de Morais, M. V. B., Martins, J. A.,
862 & Blain, G. C. (2022, 1). Evaluation of Quantile Delta Mapping as a bias-
863 correction method in maximum rainfall dataset from downscaled models in São
864 Paulo state (Brazil). *International Journal of Climatology*, *42*(1), 175–190.
865 doi: 10.1002/joc.7238